6th European Conference on Computational Mechanics (ECCM 6)
7th European Conference on Computational Fluid Dynamics (ECFD 7)
1115 June 2018, Glasgow, UK

LARGE EDDY SIMULATION OF FLOW PAST A BLUFF BODY USING IMMERSED BOUNDARY METHOD

Yongxin Chen[1], Kamal Djidjeli[2] AND Zheng-Tong Xie[3]

[1 2 3] University of Southampton
University Road, Southampton, SO17 1BJ, United Kingdom
y.chen@soton.ac.uk; kkd@soton.ac.uk; z.xie@soton.ac.uk

Key words: Immersed Boundary Method, Turbulence, LES

Abstract. An efficient and accurate finite volume incompressible flow solver with a staggered arrangement in the Cartesian grid has been developed to simulate turbulent flow past a moving bluff body. To simulate flow around a bluff body, an efficient immersed boundary method is implemented to construct geometry in the Cartesian grid, which substantially simplifies the mesh generation for complex geometries. In this paper, flow past a stationary square cylinder at Reynolds number 21,400, based on cylinder width and free stream velocity, is studied by LES with the developed immersed boundary method. The sensitivity of resolution is tested and convergence is achieved. Both experimental and numerical results are used for validation. The global aerodynamic quantities such as lift and drag coefficients and Strouhal number are in good agreement with reference data. The turbulent statistics, in particular in the shear layer and wake regions are compared rigorously with the reference data as well. The developed solver is able to accurately predict the surface force fluctuation, which is extremely challenging from a numerical point of view.

1 INTRODUCTION

The flow over a square cylinder at the Reynolds number $Re = 21,400$ based on freestream velocity U_0 and cylinder side length D was widely studied by both experiments and numerical simulations. The flow is laminar at the inlet and becomes turbulent near the leading corners of the square cylinder. The flow develops to be fully turbulent flow in further downstream and forms vorticities near the trailing corners of the cylinder.

This case was initially studied with experiment approach by Lyn and Rodi [7] and Lyn et al. [6]. Rodi and Ferziger selected this case as an international test case for a workshop held in Germany and then reported by Rodi et al. [9]. The results from several different international groups were obtained using numerical simulation with different methods, models and meshes, and presented in ERCOFTAC workshop in 1996 (archived in Direct and Large eddy simulations report [4]). In this case, although the geometry is simple and the configurations are straightforward, it still exhibits many difficulties in LES, for example, the transition problem, the estimation of the vortex formation length

in the wake region and so on [4]. Even for the first order statistics, LES has difficulties to predict properly in some regions of the domain.

The immersed boundary method is implemented in the present study to simulate the flow over an obstacle. The immersed boundary method is proven very useful in many applications and very efficient in constructing complex geometries and solving moving body problems. Despite the convenience and efficiency, it is challenging to have an accurate prediction in the near-wall region by immersed boundary method. In this study, accuracy of the immersed boundary method is assessed through examining both global integral force coefficients and the surface force distribution.

The rest of paper is organized as follows. Section 2 shows the governing equations and LES sub-grid model used. The numerical methods including flow solver and the immersed boundary method are introduced in section 3. The computational case in terms of configuration, grid sensitivity test, time averaged statistics results and discussion are presented in section 4. Finally, the relevant results are concluded in the last section.

2 Governing equations

In LES, the large-scale velocity and pressure are resolved and can be obtained from the solution of spatial filtered Navier-Stokes (NS) equations, while the small scale quantities are modelled. In the present study, the top-hat filtering operation is applied in the governing equations and the filtered incompressible NS equations and continuity equation in tensor notation are:

$$\frac{\partial \bar{u}_i}{\partial t} + \frac{\partial \bar{u}_i \bar{u}_j}{\partial x_j} = -\frac{1}{\rho}\frac{\partial \overline{p}}{\partial x_i} + \nu \frac{\partial^2 \bar{u}_i}{\partial x_j \partial x_j} - \frac{\partial \tau_{ij}}{\partial x_j} + f_i \tag{1}$$

$$\frac{\partial \bar{u}_i}{\partial x_i} = 0 \tag{2}$$

where $\bar{u}_i$ and $\bar{p}$ are filtered velocity and pressure respectively, ρ is density and ν is the kinematic viscosity, f_i represents the external body force, which is applied to satisfy the proper boundary conditions on an immersed body. The effect of small scales appears through sub-grid scale (SGS) stress term, $\tau_{ij} = \overline{u_i u_j} - \bar{u}_i \bar{u}_j$, which is modelled.

In order to solve equation 1, the SGS term τ_{ij} should be expressed in terms of the known quantities. The most commonly used SGS models are eddy eddy-viscosity models with the form:

$$\tau_{ij} - \frac{\delta_{ij}}{3}\tau_{kk} = -2\nu_t \bar{S}_{ij} = -\nu_t \big(\frac{\partial \bar{u}_i}{\partial x_j} + \frac{\partial \bar{u}_j}{\partial x_i}\big) \tag{3}$$

To quantify the subgrid eddy viscosity ν_t, mixed time scale (MTS) model [5] is used. The mixed time scale model can be expressed as:

$$\nu_t = C_{MTS} k_{es} T_S \tag{4}$$

$$T_S^{-1} = \big(\frac{\bar{\Delta}}{\sqrt{k_{es}}}\big)^{-1} + \big(\frac{C_T}{|\bar{S}|}\big)^{-1} \tag{5}$$

where $\bar{\Delta}$ is filter length scale and calculated by $\bar{\Delta} = (\Delta x \Delta y \Delta z)^{\frac{1}{3}}$. The model parameters C_{MTS} and C_T are set as default to 0.05 and 10 respectively. $|\bar{S}| = \sqrt{2\bar{S}_{ij}\bar{S}_{ij}}$. k_{es} is SGS turbulent energy and computed as:

$$k_{es} = (\bar{u}_i - \tilde{\bar{u}}_i)^2 \tag{6}$$

The notation $(\tilde{\bar{u}})$ denotes the test filtering option for local velocity, for which the weighted average is used.

3 Numerical methods

3.1 Flow solver

The second order Adam-Bashforth method [13] is used to discretize incompressible NS equations in time and it can be formulated as:

$$\frac{u^* - u^n}{\Delta t} = \frac{3}{2}H^n - \frac{1}{2}H^{n-1} + f \tag{7}$$

$$\Delta t \frac{1}{\rho}\frac{\partial^2 p^{n+1}}{\partial x_i^2} = \frac{\partial u^*}{\partial x_i} \tag{8}$$

$$u^{n+1} = u^* - \frac{\Delta t}{\rho}\frac{\partial p^{n+1}}{\partial x_i} \tag{9}$$

where superscript n and $n+1$ denote the current and next time step and $*$ is intermediate time step. f is external body force term which enforces the immersed boundary condition for u^*. H represents the rest of terms in NS equation except for the pressure term:

$$H = -\frac{\partial u_i u_j}{\partial x_j} + \frac{\partial}{\partial x_j}\big[(\nu_t + \nu)\big(\frac{\partial u_i}{\partial x_j} + \frac{\partial u_j}{\partial x_i}\big)\big] \tag{10}$$

The governing equations are discretized in space using second order central differencing finite volume method, where the variables are stored in a fully staggered arrangement in the Cartesian grid. In each iteration of flow solver, all variables are advanced in time and split into two steps. In the step 1, by dropping the pressure term, an intermediate velocity, which is not divergence-free, is obtained by explicit time integration in Equation 7. In step 2, the divergence free condition is applied in the velocity field to get pressure field in Equation 8 and then the pressure field is used to project intermediate velocity field to new velocity field in Equation 9, which satisfies the divergence free condition. In the present study, the pressure Poisson in Equation 8 is solved by using the Gauss-Seidel iterative method. In order to increase the convergence speed, the multigrid method [8] is used.

3.2 Immersed boundary method

The occurrence of bodies in the fluid is to change the distribution of fluid field in near boundary region. For example, the flow speed reduces to zero on the boundary of a stationary body. This effect can be achieved by introducing an external body force term

f, which enforces a proper boundary condition, in NS equations in the Cartesian grid flow solver to simulate flow past an immersed body. In the present study, the immersed boundary method of Yang and Balaras [14] is used.

An arbitrary shape can be represented by a series of markers on the interface. The signed distance function ψ can be used to distinguish which phase that each grid point belongs to. The signed distance function ψ is positive if the grid point is in fluid phase while negative in the solid phase. By using signed distance function, all the grid points can be classified into three groups: (1) solid points with $\psi < 0$, (2) fluid points with $\psi > 0$ and there is no direct neighbour solid point, and (3) forcing points are points in the fluid and with at least one direct neighbour solid point.

The body force is set to zero at all the fluid points. At solid points, the body force is chosen to make velocity equal to body motion velocity. For example, if a body is stationary, the body force is chosen to make velocity to 0. At forcing points, the velocity is expressed as the result of linear interpolation from surrounding points in the normal direction of interface towards fluid, which represents velocity linear distribution in the viscous sub-layer. The linear interpolation needs three points in 2D and four points in 3D and each interpolation stencil includes a point on the interface and other points are in the fluid phase. The interpolation stencil in 2D can be seen in the following figure. To avoid ambiguity and difficulty in choosing linear interpolation stencil, where other forcing points could be included, an iterated interpolation step by Busse et al. [2] is used.

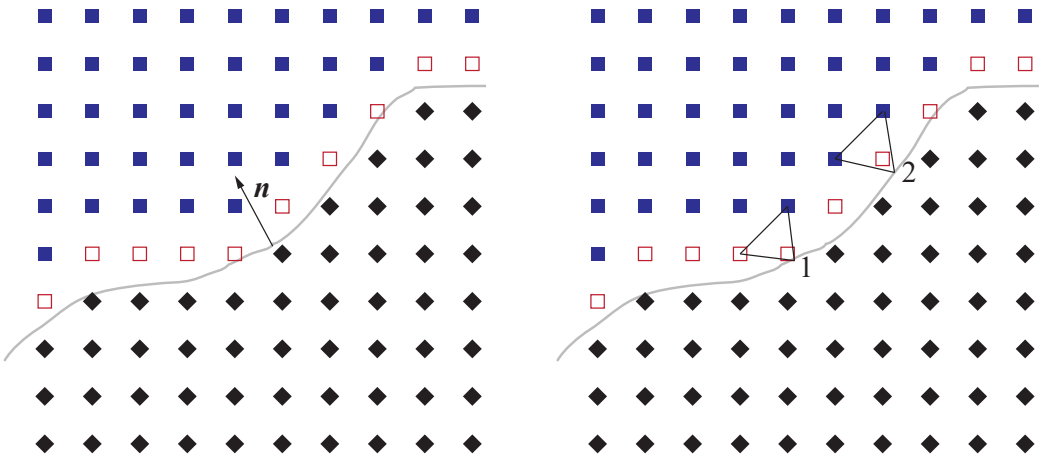

Figure 1: Left: Classification of grid points: fluid points (blue squares), solid points (black diamonds) and forcing points (red squares). The black curve is the interface of immersed body and the normal direction towards fluid. Right: Examples of linear interpolation stencil in 2D. Stencil 1 includes two forcing points and one fluid point while stencil 2 includes one forcing point and two fluid points. This figure is redrawn from [2].

4 Computational case

4.1 Configuration and grid sensitivity

The schematic of the computational domain is presented below. The characteristic length is the side length D of square cylinder. The simulation is performed on the Cartesian grid. The centre of square cylinder is located at the origin. The computational domain size is $25D \times 14D \times 2D$ in the stream-wise, cross-stream and span-wise directions respectively. To reduce the computational cost, the span-wise length is set to $2D$ and the length of the domain must be larger than the biggest eddy. Trias et al. [12] calculated two-point correlations of span-wise velocity and other variables by direct numerical simulation in the case of flow past a square cylinder at a Reynolds number 22,000. The correlation results show the values decrease to zero at the distance less than 1D from the centre to edge. It indicates the $2D$ span-wise length is sufficient in this configuration. The length from the centre of cylinder to the inlet and outlet are $5D$ and $20D$ respectively. The length to the top and bottom boundaries is $7D$. The axis of the cylinder is aligned with the span-wise direction. The stream-wise, cross-stream and span-wise directions are aligned with x, y and z axes and indexed as 1, 2 and 3 respectively. A sponge layer, which generally decays the fluctuation, is applied in the last $5D$ at the outlet region. The correspondent velocity components are u, v and w respectively. This convention is used for the rest of this paper.

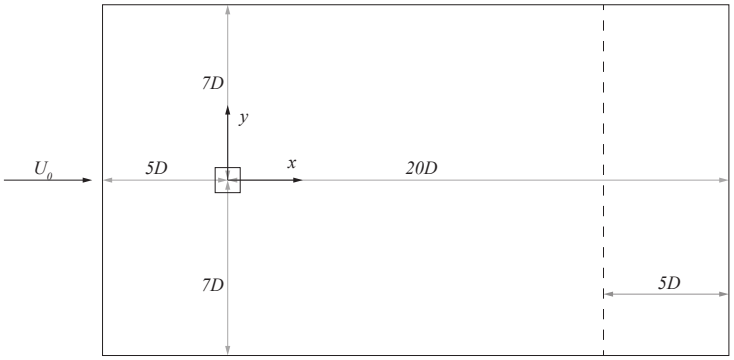

Figure 2: Domain schematic.

Regarding the boundary conditions, an uniform constant velocity is imposed at the inlet, $\mathbf{u} = (U_0, 0, 0)$. The outlet boundary condition is a zero gradient condition, $\partial u_i/\partial x = 0$. Symmetric boundary condition is used in top and bottom planes, $\partial u/\partial y = \partial w/\partial y = 0$ and $v = 0$. Zero gradient boundary condition is imposed for pressure at these four planes. Periodic boundary condition is used in span-wise direction for both velocity and pressure. No slip boundary condition is applied to the square cylinder by the current immersed boundary method.

The objective of the present study is to validate the current immersed boundary method in terms of global aerodynamic quantities, turbulence statistics and surface force fluctuations. In the present study, the time step Δt is chosen to 0.001 and this was chosen to keep the CFL number ($U\Delta t/\Delta x$) less than 1. 10^5 time steps are used to initialize and

they are equivalent to 100 time unit based on tU_0/D. At least 25 vortex shedding cycles are used to compute the aerodynamic characteristics, which are adequate to perform statistics analysis.

Three sets of grid meshes are used to test the grid sensitivity of the simulation. Three cases, which are coarse, medium and fine resolution, consist of 256×256, 288×288 and 320×320 meshes respectively with 100, 110 and 120 points to resolve per side of the cylinder in the lateral plane. An uniform mesh is used in the body region to obtain good quality and stretched mesh is used in other regions where the mesh is finer in near cylinder region while is coarser and stretched in the far region. The maximum stretch ratio is 1.08. The grid number in span-wise direction is 32 for $2D$ width and equispaced. This span-wise grid resolution and length ratio (16/D) is suggested in the previous LES study [4]. The computation results of global aerodynamic quantities, i.e. lift, drag and Strouhal number and span-wise averaged statistics result at shear layer region against both numerical and experimental data for three meshes are shown in the following parts.

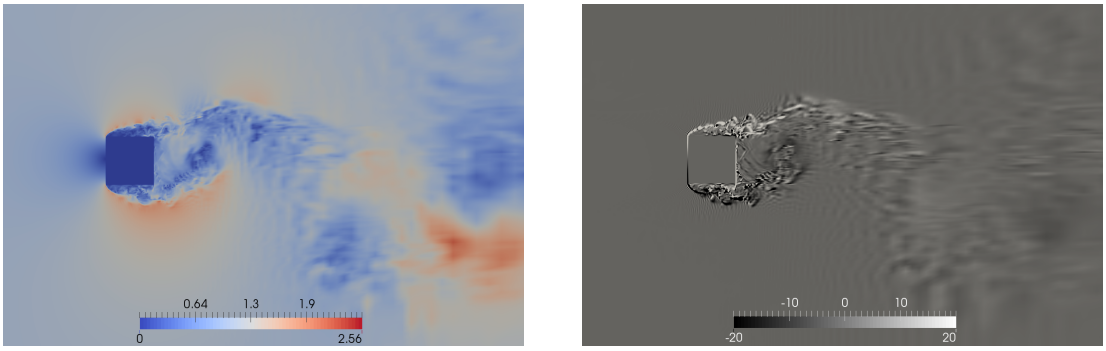

Figure 3: Snapshots of non-dimensional velocity magnitude ($|\mathbf{u}|/U$, left) and span-wise vorticity ($\omega_z D/U_0$, right) fields at $tU_0/D = 260$. The vorticity field is rescaled from -20 to 20.

The snapshots of instantaneous flow visualization are shown in Figure 3 where the flow is uniform at the upstream inlet and becomes turbulent when the flow past the sharp corners in leading edge. Flow separation is formed and vortices are generated from the leading edge corners and then fully developed to turbulent flow. Vortices are asymmetrically shed in the wake region and convected to downstream.

Table 1: Comparison of global quantities in different meshes

Case	Resolution	St	$\overline{C_D}$	$C_{D\ r.m.s}$	$C_{L\ r.m.s}$
Coarse	$256 \times 256 \times 32$	0.140	2.17	0.15	1.41
Medium	$288 \times 288 \times 32$	0.135	2.21	0.17	1.36
Fine	$320 \times 320 \times 32$	0.135	2.18	0.18	1.31
LES [3]	-	0.131-0.140	2.19-2.24	0.14-0.273	1.27-1.71
DNS [12]	$1272 \times 1174 \times 216$	0.132	2.18	0.205	1.15-1.79

To validate the convergence result, previous LES and DNS are used. LES results are from the grid convergence test result of Cao et al. [3], by using different schemes and meshes, and DNS is from Trias et al. [12]. The convergence of global quantities is listed in Table 1. In the present study, the lift and drag forces are computed by integrating the body force. Overall, the present results are in the range of reference data and convergence is achieved. One should note that the fluctuating forces show greater discrepancy than other parameters and this discrepancy is primarily due to the sensitivity of a relatively short span-wise length. According to Cao et al. [3], the span-wise length is essential to reduce fluctuating forces and a dramatic reduction is found when the span-wise length is extended to $14D$ as vortices with large different phases are shed.

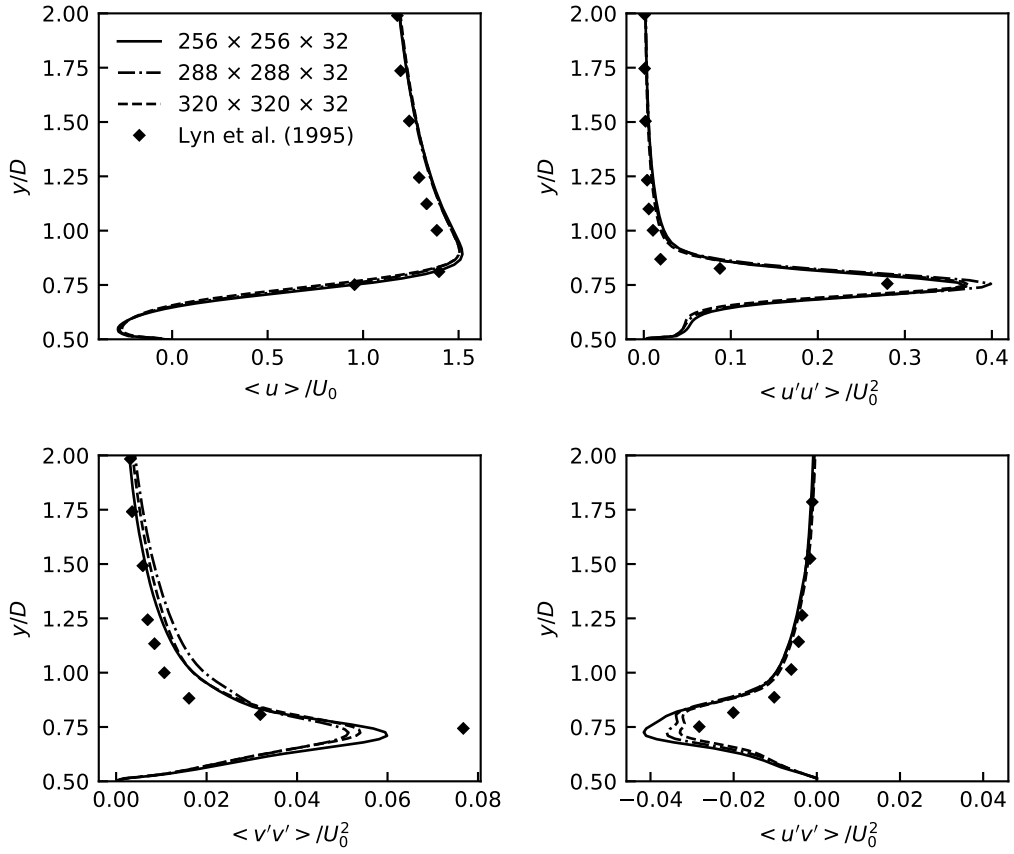

Figure 4: Grid sensitivity test in the shear layer region $x/D = 0$. Mean streamwise velocity (top left), $< u'u' >$ (top right), $< v'v' >$ (bottom left), $< u'v' >$ (bottom right).

The time- and span-averaged statistics including non-dimensional mean stream-wise velocity and Reynolds shear stress in the shear layer at $x/D = 0$ are shown in Figure 4. To compare the results, the experimental data of Lyn et al. [6] is used. In the comparison, $<\cdot>$ denotes time averaged quantity. As can be seen from comparison, the present results from three meshes are in good agreement with experimental data and the difference between each mesh is small. In this case, it can be considered that the solution is independent of the mesh resolution.

4.2 Results and discussion

Figure 5 shows the statistics profiles in the horizontal wake centreline. It should be noted that the upstream turbulence intensity is around 2% in the experiment of Lyn et al. [7], which should be taken into account for more cautious comparisons.

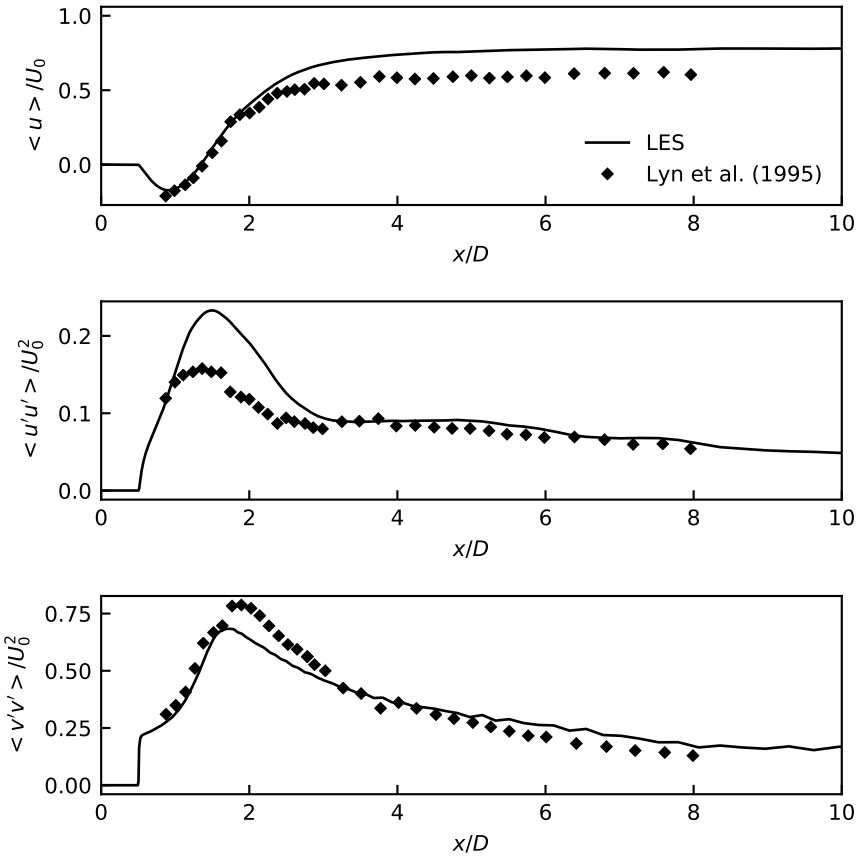

Figure 5: Comparisons of statistics in horizontal centreline. From top to bottom are time averaged non-dimensional stream-wise velocity $< u >$, Reynolds stresses $< u'u' >$ and $< v'v' >$. The solid line is the present LES result performed on $320 \times 320 \times 32$ mesh as the following figures.

The prediction of vortex formation length is a key factor to validate the simulation results. This value is obtained from zero cross point, i.e. $< u > /U_0 = 0$ on the centreline plane. From the mean stream-wise velocity profile, the prediction of vortex formation length is accurately obtained by the current solver with the fine mesh. The mean stream-wise velocity is over-predicted in the wake region, as found in many LES studies [4, 3] and DNS study [12]. Sohankar et al. [10] suggested this discrepancy is possibly due to the insufficient grid resolution in span and lateral section in far wake region. Improved grid resolution using DNS [12] or longer span-wise length ($14D$) using LES [3] both show better agreement with experimental results. For Reynolds stresses, peak value of $< u'u' >$ is over-predicted and $< v'v' >$ is slightly under-estimated in the wake. It should be noted

that three meshes have only small difference in the resolution on the side of the cylinder (100, 110 and 120) and stretch ratio in the wake region. However, the discrepancy in prediction of $< u'u' >$ is both found between three meshes and in the comparison with experimental data. The relative error of $< u'u' >$ between experiment and LES for the peak in near wake region ($x/D < 3$) is about 25%. The location of velocity fluctuation peak values are within the vortex formation region, where the fluid is blocked by the obstacle and has a much slower motion than shear layer regions. In the near wake region, the fluid is entrained from shear layer to the centreline and the vertical velocity is the principal component over the stream-wise velocity. The velocity component with a smaller magnitude is more sensitive to the fluctuation and this is consistent to the LES result. Apart from the difference in the over-prediction of peak values of velocity fluctuation, both Reynolds stresses have a good agreement in the far wake region ($x/D > 3$).

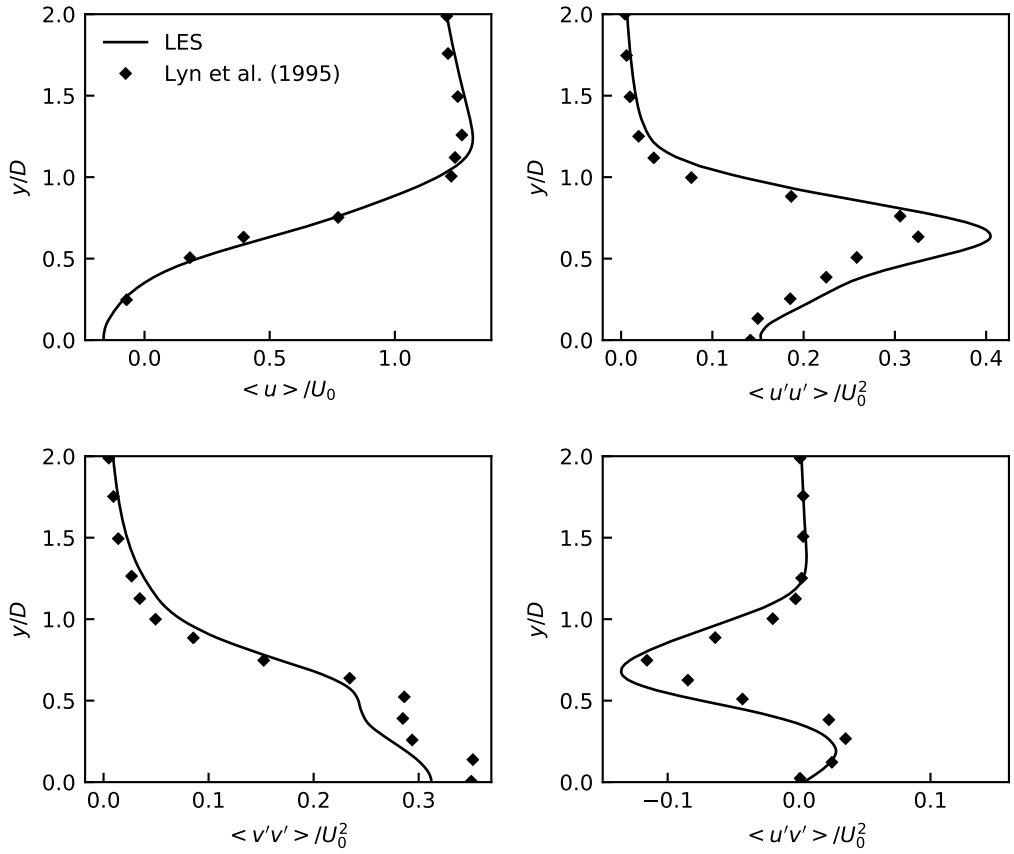

Figure 6: Comparison of shear layer in the wake region $x/D = 1$.

Figure 6 shows the time and span averaged statistics results at $x/D = 1$ in the wake region. As can be seen, the present results have good agreement with the experimental data. In the $0.5 < y/D < 0.75$ region where separation is formed, the Reynolds stresses $< u'u' >$ and $< u'v' >$ are slightly shifted from the experiment data and the results are slightly over-estimated. The overestimation in the near wake region is consistent with previous findings in the horizontal centreline.

Figure 7 shows the distribution of pressure coefficient C_P and root mean square (r.m.s) of pressure coefficient $C_{P\ r.m.s}$ along the circumferential direction of cylinder. C_P and $C_{P\ r.m.s}$ can be defined as:

$$C_P = \frac{1}{N}\frac{\Sigma_{i=1}^{N}(p_i - p_\infty)}{\frac{1}{2}\rho U_0^2},\ C_{P\ r.m.s} = \sqrt{\frac{1}{N}\frac{\Sigma_{i=1}^{N}(p_i - \overline{p})^2}{\frac{1}{2}\rho U_0^2}} \tag{11}$$

where p_i and $\overline{p}$ are instantaneous and mean pressure respectively, p_∞ is the reference pressure, $p_i - \overline{p}$ is pressure fluctuation. The experimental data by Bearman et al. [1] at Reynolds number in the range from 5.8×10^3 to 3.2×10^4 is used to validate the present results.

Since the staggered mesh and immersed boundary method are used, the pressure points are not always coincident to the cylinder's surface. Hence, the extrapolation should be used to estimate the surface pressure from the fluid. The pressure on the surface is p_S and p denotes the correspondent nearest pressure point in the fluid. The extrapolation from fluid pressure to surface pressure can be simply expressed as $p_S = p$. However, this expression is with first order accuracy. Since the body force is implemented in both inside and first grid outside the immersed boundary, hence the fluid pressure is different from surface pressure, which is affected by the body force field. In order to obtain a second order accuracy, the Taylor expansion of fluid pressure point is used to obtain the surface pressure:

$$p_S = p - \frac{\partial p}{\partial n}d \tag{12}$$

where d is distance between the nearest point and surface, $\partial P/\partial n$ is the pressure directional derivative along the surface normal direction n.

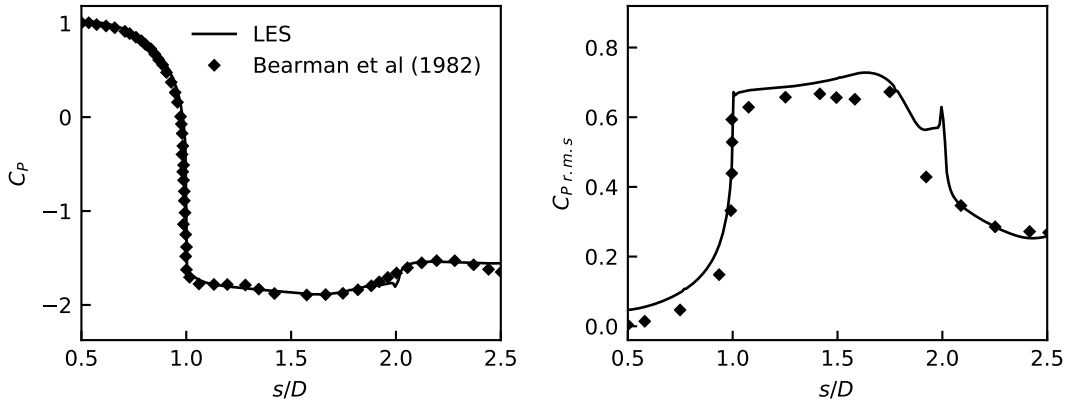

Figure 7: Comparison of distribution of C_P (left) and $C_{P\ r.m.s}$ (right).

The pressure coefficient distribution from the LES is in a very good agreement with experimental data and r.m.s of pressure coefficient is in a promising comparison. The level of pressure fluctuation at the frontal surface ($0.5 < s/D < 1.0$) is higher than the

measurement. The higher level of pressure fluctuation on the frontal surface is found when the turbulence intensity increases [11]. This indicates the turbulence is over-estimated and it is possibly due to the computational grid and central difference scheme which introduces oscillation on the frontal surface.

5 Conclusion

A finite volume fluid solver with immersed boundary method has been developed. The benchmark case flow past a stationary square cylinder at a Reynolds number 21,400 based on the cylinder's side is studied. Three meshes are used to conduct grid sensitivity test and the convergence of grid is achieved. The time averaged mean quantities, such as lift, drag and stream-wise velocity, and distribution of pressure coefficient are well estimated. The drag and lift fluctuations are less accurately estimated than other global quantities and mainly due to the short span-wise domain length. The velocity fluctuations in the near wake is found to be very sensitive to different grid resolution. In particular, the peak value of velocity fluctuations show a less accurate prediction in the near wake region and this can be owing to various factors, such as SGS models, numerical schemes and resolution. Overall, the current immersed boundary method is able to produce good estimation in simulating flow past bluff body in turbulent flow.

REFERENCES

[1] Bearman, P., and Obasaju, E. An experimental study of pressure fluctuations on fixed and oscillating square-section cylinders. *Journal of Fluid Mechanics 119* (1982), 297–321.

[2] Busse, A., Lützner, M., and Sandham, N. D. Direct numerical simulation of turbulent flow over a rough surface based on a surface scan. *Computers & Fluids 116* (2015), 129–147.

[3] Cao, Y., and Tamura, T. Large-eddy simulations of flow past a square cylinder using structured and unstructured grids. *Computers & Fluids 137* (2016), 36–54.

[4] Chollet, J.-P., Voke, P. R., and Kleiser, L. Direct and large-eddy simulation ii.

[5] Inagaki, M., Kondoh, T., and Nagano, Y. A mixed-time-scale sgs model with fixed model-parameters for practical les. *Journal of fluids engineering 127*, 1 (2005), 1–13.

[6] Lyn, D. A., Einav, S., Rodi, W., and Park, J.-H. A laser-Doppler velocimetry study of ensemble-averaged characteristics of the turbulent near wake of a square cylinder. *Journal of Fluid Mechanics 304*, -1 (1995), 285.

[7] Lyn, D. A., and Rodi, W. The flaping shear layer formed by flow separation from the forward corner of a square cylinder. *Journal of Fluid Mechanics 267* (1994), 353–376.

[8] Press, W. H. *Numerical recipes 3rd edition: The art of scientific computing*. Cambridge university press, 2007.

[9] Rodi, W., Ferziger, J., Breuer, M., and Pourquie, M. Status of large eddy simulation: results of a workshop. *Transactions-American Society of Mechanical Engineers Journal of Fluids Engineering 119* (1997), 248–262.

[10] Sohankar, A., Davidson, L., and Norberg, C. Large eddy simulation of flow past a square cylinder: comparison of different subgrid scale models. *Journal of Fluids Engineering 122*, 1 (2000), 39–47.

[11] Tamura, T., and Ono, Y. Les analysis on aeroelastic instability of prisms in turbulent flow. *Journal of wind engineering and industrial aerodynamics 91*, 12-15 (2003), 1827–1846.

[12] Trias, F., Gorobets, A., and Oliva, A. Turbulent flow around a square cylinder at reynolds number 22,000: A dns study. *Computers & Fluids 123* (2015), 87–98.

[13] Xie, Z., Voke, P. R., Hayden, P., and Robins, A. G. Large-eddy simulation of turbulent flow over a rough surface. *Boundary-layer meteorology 111*, 3 (2004), 417–440.

[14] Yang, J., and Balaras, E. An embedded-boundary formulation for large-eddy simulation of turbulent flows interacting with moving boundaries. *Journal of Computational Physics 215*, 1 (2006), 12–40.